RapidScat Diurnal Cycles Over Land

Aaron C. Paget, *Member, IEEE*, David G. Long, *Fellow, IEEE*, and Nathan M. Madsen, *Member, IEEE*

***Abstract*—RapidScat, which is a Ku-band scatterometer mounted on the International Space Station, observes the Earth's surface in a non-sun-synchronous orbit allowing for different local time-of-day (LTOD) observations as the orbit progresses. The unique orbit and different LTOD observations provide surface observations that are composited to describe the diurnal variability of Ku-band normalized backscatter (σ^0) measurements over land globally. Previous sun-synchronous scatterometers providing twice-daily surface observations have been used to demonstrate some diurnal changes in σ^0 in several regions globally, but instrument cross-calibration concerns prevent identifying diurnal changes by combining σ^0 observations from multiple sensors. As a result, the full extent of diurnal changes to σ^0 has not been determined until now. In this paper, RapidScat is used to identify diurnal changes to σ^0 globally. Vegetation type is discussed with respect to the diurnal changes in σ^0 regionally. The global diurnal changes to σ^0 are discussed with emphasis on the Amazon, Congo, and Upper Danube river regions. Diurnal cycles are described that could not previously be identified with sun-synchronous instruments. Global means and the magnitude of the diurnal cycle are discussed. With the diurnal changes identified and quantified, RapidScat can be used for future cross-platform calibrations using land targets.**

***Index Terms*—Amazon, Congo, diurnal cycle, International Space Station (ISS), Ku-band, land surface observations, QuikSCAT, RapidScat, scatterometer, scatterometry.**

I. Introduction

PAST satellite-based scatterometers in sun-synchronous orbits have been used to observe land and water surfaces for several decades, observing midlatitude areas during one ascending and one descending pass at an oblique angle daily, which is roughly 12 h apart (see Table I). Diurnal changes in the scatterometer backscatter signal have been sampled and analyzed at these 12-h intervals [1]–[4] with results similar to Fig. 1; however, until recently, satellite-based scatterometers have not been able to observe the full diurnal cycle with sufficient spatial and temporal sampling to account for changes in seasonal vegetation and surface changes. The non-sun-synchronous precipitation radar on the Tropical Rainfall Measuring Mission (TRMM) has observed diurnal Ku-band backscatter [5], but the near-nadir viewing angle and much smaller footprint of 4.3–5 km for the Precipitation Radar [6], [7] requires several months of observations before the diurnal signal can be resolved for a given location, and TRMM observations are not easily comparable to standard scatterometers that have larger incidence angles.

The RapidScat scatterometer [8], [9], now flying on the International Space Station (ISS) and operating in the Ku-band (13.4 GHz), employs equipment similar to the SeaWinds instruments [10], [11], with a similar footprint, frequency, and surface incidence angle (see Table I). The unique orbit of the ISS platform allows for surface observations at different times of the day spread over approximately 22 days for a single instrument [see Fig. 2(a)], with some days having multiple views of a given area [see Figs. 2(b) and 3(a)] and extended periods of time without observations [see Figs. 2(c) and 3(b) and (c)]. The main goals of this research are to identify the diurnal cycle of the scatterometer backscatter signal as observed by RapidScat and to discuss the potential effects of vegetation and ground cover on the signal.

II. Background

RapidScat, which is a rotating pencil-beam scatterometer, alternatingly emits both horizontal polarization (HH) and vertical polarization (VV) microwave signals directed at the Earth's surface with a range of incidence angles, 44–54° for HH and 51–61° for VV, depending on the altitude and attitude of the ISS. RapidScat observes the surface in a helical pattern about the ground track [see Fig. 2(b)]. The rotation provides fore and aft observations at various azimuthal angles. The surface scatters the signal, and the portion of the signal scattered back to the instrument, i.e., the backscatter, is measured and used to interpret surface characteristics over land and retrieve ocean vector winds over water. Different land types, soil moisture, vegetation, and infrastructure modify the signal over land with the value of the normalized backscatter, i.e., σ^0, normally in the range of -25 to -3 dB. The values of σ^0 over water are normally less than that over land and vary between -40 and -12 dB.

For land, vegetation changes, such as leaf moisture and dew, can influence scattering properties on a diurnal cycle. These changes have been studied with microwave radiometer data [12]–[14] and twice-daily observations using scatterometers [3], [4], [15]–[17] in limited studies of the diurnal evolution.

The RapidScat instrumentation largely comes from the original SeaWinds engineering test instrument with the key exception of the antenna, which was redesigned for use on the ISS platform. SeaWinds operated on ADEOS-II and QuikSCAT (see Table I). SeaWinds on QuikSCAT (hereafter referred

Manuscript received April 13, 2015; revised October 13, 2015; accepted December 8, 2015. Date of publication January 27, 2016; date of current version April 27, 2016.

A. C. Paget is with the Department of Electrical and Computer Engineering and the Microwave Earth Remote Sensing Laboratory, Brigham Young University, Provo, UT 84602 USA, and also with the Department of Marine Sciences, University of Connecticut, Groton, CT 06340 USA (e-mail: aaroncpaget@gmail.com).

D. G. Long is with the Department of Electrical and Computer Engineering and the Microwave Earth Remote Sensing Laboratory, Brigham Young University, Provo, UT 84602 USA (e-mail: long@ee.byu.edu).

N. M. Madsen was with the Department of Electrical and Computer Engineering, Brigham Young University, Provo, UT 84602 USA. He is now with Rincon Research Inc., Tucson, AZ 85711 USA (e-mail: nmmadsen@mers.byu.edu).

Color versions of one or more of the figures in this paper are available online at http://ieeexplore.ieee.org.

Digital Object Identifier 10.1109/TGRS.2016.2515022

TABLE I
KU-BAND SCATTEROMETERS WITH MISSION AND INSTRUMENT DETAILS

	SASS	NSCAT	SeaWinds	SeaWinds	OSCAT	HY-2A	RapidScat
Frequency (Ku-band)	14.6 GHz	13.995 GHz	13.6 GHz	13.6 GHz	13.6 GHz	13.256 GHz	13.6 GHz
Antenna azimuths							
Polarizations	VV and HH	VV and HH	VV-outer HH-inner	VV-outer HH-inner	VV-outer HH-inner	VV-outer HH-inner	VV-outer HH-inner
Beam resolution	Fixed Doppler	Variable Doppler	Pencil-beam	Pencil-beam	Pencil-beam	Pencil-beam	Pencil-beam
Resolution (σ^0)	Normally 50 km	25 km	Egg: 25x36 km Slice: 6x25 km	Egg: 25x36 km Slice: 6x25 km	Egg: 30x68 km Slice: 5x30 km	Outer beam 37 x 26 km Inner beam 33 x 23 km	Egg: 26x37 km Slice:8x26 km
Swath (km)	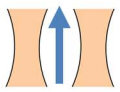 ~750 ~750	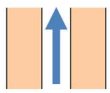 600 600	 1400, 1800	 1400, 1800	 1400, 1836	 1350, 1700	 900, 1100
Incidence angles	0° - 70°	12° - 60°	46° & 54.4°	46° & 54.4°	49° & 57°	41.36° & 48.44°	49° & 56°
Daily coverage	Variable	78%	92%	92%	>90%	90%	65% between 58°N and 58°S
Mission & Dates	SeaSat 6/1978-10/1978	ADEOS-I 8/1996 - 6/1997	QuikSCAT 6/1999 - 11/2009	ADEOS II 1/2002 - 10/2002	OceanSat-2 10/2009 -2/2015	8/2011 -	International Space Station 10/2014 -
Orbit type	Sun-synchronous	Sun-synchronous	Sun-synchronous	Sun-synchronous	Sun-synchronous	Sun-synchronous	Non sun-synchronous
Ascending equatorial crossing local time	6:00 AM & 12:00 PM	6:30 AM	6:00 AM	10:30 PM	12:00 AM	6:00 PM	Various
Orbit inclination	108°	98.616°	98.6°	98.62°	98.28°	99.3°	51.65°
Altitude (nominal)	805 km	803 km	800 km	802.9 km	720 km	970 km	375 – 435 km
Period	100.7 min	101 min	101 min	101 min	99.31 min	104.45 min	92.69 min

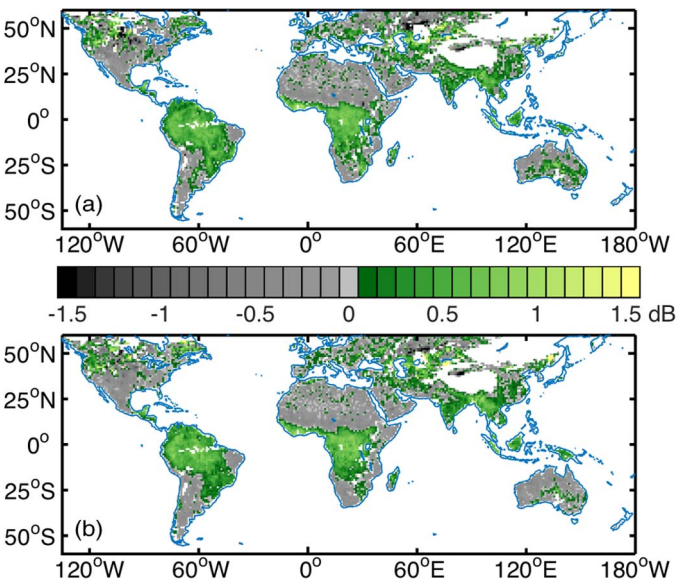

Fig. 1. Differences in median σ^0 for morning and evening equatorial cross times from 1 October 2008 to 4 February 2009 as observed by QuikSCAT for (a) horizontal polarization (HH) and (b) vertical polarization (VV). Positive values indicate that morning observations are higher than evening observations.

to as QuikSCAT) operated for over ten years as a rotating pencil-beam scatterometer in a sun-synchronous orbit and provided steady and reliable σ^0 observations. Observations from RapidScat help identify the entire diurnal cycle that was only partially observed by QuikSCAT. Because of the similar instrumentation between the sensors, QuikSCAT observations are included in this study to help identify and quantify the diurnal σ^0 changes observed by RapidScat.

III. DATA

RapidScat was launched to the ISS on 21 September 2014 as part of the SpaceX CRS-4 mission and started transmitting data in early October 2014. The ISS orbit enables surface observations by RapidScat within an equatorial band of $\pm 51.6^\circ$ latitude. The ISS orbit permits observations of a full 24 h of the LTOD for any point within the equatorial band approximately every two months for ascending or descending pass. For a 1° grid, gaps in the LTOD observations are no larger than 3.4 h, and 90% of the grid elements are within a maximum observational time gap of less than 79 (95) min for VV (HH) [see Fig. 3(b) and (c)]. As RapidScat rotates, observations are

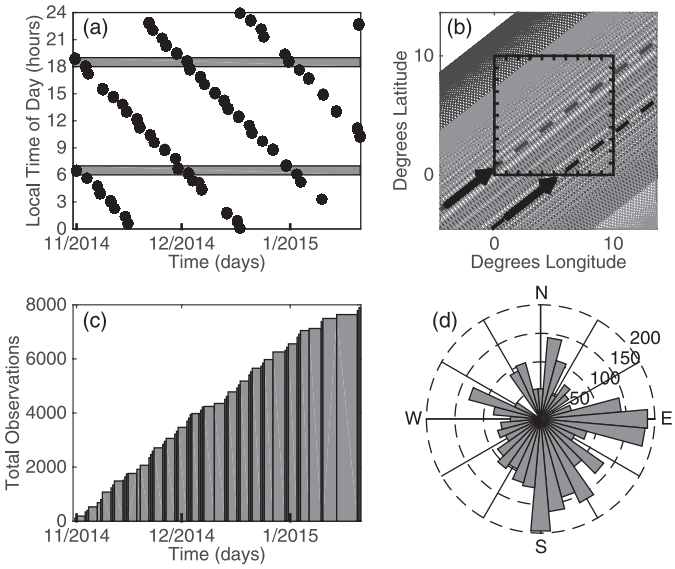

Fig. 2. (a) Dates and local time of day (LTOD) for observations in a $1^\circ \times 1^\circ$ region at 0°N and 100° E in Sumatra. Black dots indicate RapidScat observations, and gray bars indicate observation times from the QuikSCAT wind mission. (b) Two ascending ground tracks of RapidScat (black dashed line) 15 revolutions (about 23 h) apart with the helical observations around the first pass (dark gray) and the second pass (light gray) for a sample region. Arrows indicate direction of orbital motion. (c) Cumulative histogram by time of RapidScat σ^0 observations for the $1^\circ \times 1^\circ$ region in Sumatra. Column width indicates the amount of time between observational passes. (d) Histogram of the RapidScat σ^0 ascending observations binned by 10° azimuth relative to north for a $1^\circ \times 1^\circ$ region at 0° N and 100° E in Sumatra.

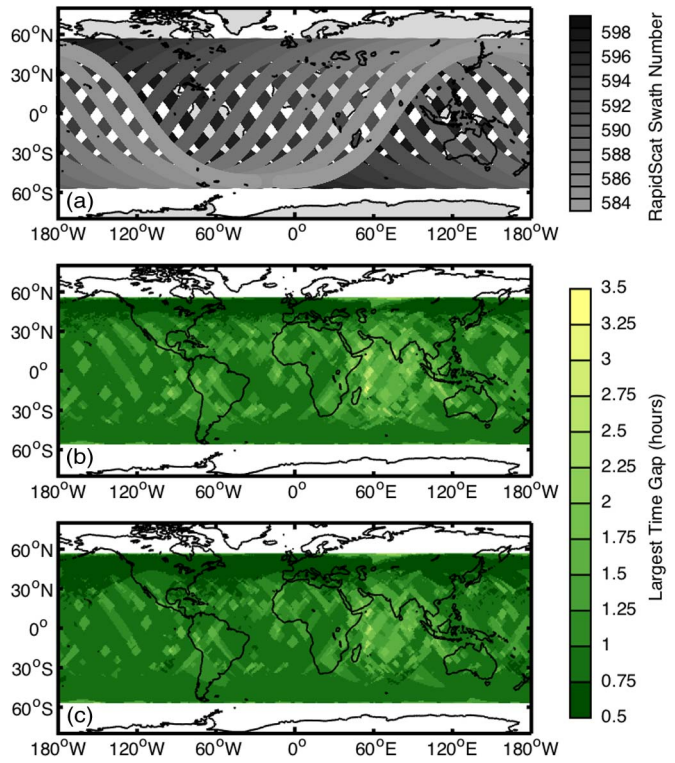

Fig. 3. (a) Full RapidScat swaths for 16 full orbits (approximately one day), where swath 584 and 599 partially overlap approximately 23 h apart. (b) Largest time gap in the composite LTOD for HH polarization with ascending and descending passes combined. (c) Largest time gap in the composite LTOD for VV polarization with ascending and descending passes combined.

obtained from most azimuth angles except within a small range to avoid the imaging part of the ISS [see Fig. 2(d)]. The missing azimuth angles are relative to the ISS, and changes in the ISS orientation with respect to north change the cardinal orientation of the missing angles. Combining ascending and descending passes provides coverage of all azimuthal angles.

In this paper, the RapidScat data are extracted from 1 November 2014 to 22 January 2015 and include all grid-cell (or "egg" as the elliptical surface footprint is sometimes described) backscatter measurements that meet a quality assessment of no bad-quality flags. All values meeting these criteria are used in the analysis. The short analysis period minimizes the influence of seasonal changes to the signal [18]. To isolate land from water, a 1° land/water mask is used to eliminate any grid cells containing large bodies of water. The static land/water mask is based on the Global Self-consistent, Hierarchical, High-resolution Geography database. The land/water mask was created by mapping the coastline (in latitude and longitude) onto a $0.01^\circ \times 0.01^\circ$ grid and then filled using standard image-filling techniques. The land/water mask was further processed into the $1^\circ \times 1^\circ$ grid used in this study with a conservative land analysis requiring all of the values from the higher resolution grid to be considered land in this land-only analysis. Some land coastal observations are not included in this analysis as a result of this conservative land mask; however, land/water signal contamination is also limited as a result.

The data for QuikSCAT diurnal change comparisons used in this paper are extracted from 1 November 2008 to 22 January 2008. These data are also used for accounting for azimuthal variations. Additional National Aeronautics and Space Administration (NASA) scatterometer (NSCAT, a fan-beam scatterometer) [5] data are used to account for incidence angle variations in RapidScat σ^0 caused by the changes in the altitude and attitude of the ISS compared with QuikSCAT [19].

The 2-m air temperature, land surface skin temperature, and snow depth are used to limit the time analysis to frost-free and freeze-free events. The data come from the European Center for Medium-Range Forecasts (ECMWF) ERA Interim, Daily step 0 that is available every 6 h. The dates for the ECMWF cover the same time period as the RapidScat and QuikSCAT observations used in this analysis.

To identify the type of ground cover and vegetation dominant in the region, the University of Maryland 1° Advanced Very High Resolution Radiometer (AVHRR) Global Land Cover Classification (GLCC) mask is used. The mask divides the RapidScat area of coverage into 11 defined regions (see Table II).

IV. Methodology

Global and selected regional analyses are provided, although the methodology slightly differs between how the regions are defined. For the global analysis, the globe is divided into a $1^\circ \times 1^\circ$ global grid corresponding to the land/water and the GLCC masks (see Fig. 4). For the $1^\circ \times 1^\circ$ global grid, observations are binned with a drop-in-the-bucket technique where the center of the observations identifies the assigned bin. All RapidScat and QuikSCAT observations are referenced to the

TABLE II
UNIVERSITY OF MARYLAND 1° AVHRR GLCC TYPES WITH CORRESPONDING NUMERICAL IDENTIFIERS

Identifier	Land Cover Classification
1	Broadleaf Evergreen Forest
2	Coniferous Evergreen Forest and Woodland
3	High Latitude Deciduous Forest and Woodland
4	Tundra
5	Mixed Coniferous Forest and Woodland
6	Wooded Grassland
7	Grassland
8	Bare Ground
9	Shrubs and Bare Ground
10	Cultivated Crops
11	Broadleaf Deciduous Forest and Woodland
12	Other

ERA-Interim values for 2-m air temperature, land surface skin temperature, and snow depth for the nearest time and the corresponding spatial grid element. Only observations with the 2-m air temperature and the land surface skin temperature both above 2 °C and with zero snow depth are included in the analysis to eliminate possible aliasing of the freeze-thaw cycle on the analysis of the diurnal signal.

From the observations in the global $1^\circ \times 1^\circ$ grid, the Upper Danube river region is defined by analyzing individual grid cells for similar mean σ^0 and similar variations in the diurnal cycle. Land surface coverage is not a consideration in identifying this region. Temperature and snow depth limit the number of observations; however, sufficient observations are available for this analysis.

The Amazon and Congo regions are also included in the analysis, with the regions defined using the same approach as previous studies to maintain consistency with previous analyses. The Amazon region has been extensively studied in the past [5], [15], [19]–[22] and has been used as a calibration region for scatterometer calibration [5], [19], [23]–[26]. The Amazon and Congo region masks are generated by averaging σ^0 over the QuikSCAT mission into a high-resolution spatial grid and selecting grid points with averages within half a decibel of a mean response for the region of interest [24]. The mean response is chosen by iteratively generating a mask and then using that mask to calculate a new mean response. The first mean response is taken as the average σ^0 at the locations specified in [27] for the Amazon and the Congo. For an observation to be included in the regional analysis, the observation cell center must be contained within the defined region in which the vegetation is largely homogeneous.

The ISS does not have a strictly controlled orbit altitude, and the attitude of the ISS occasionally changes. Changes in the attitude and altitude of the ISS affect the incidence angle of the backscatter observations. The changes in σ^0 caused by the incidence angle variations are accounted for using a linear σ^0 additive factor based on the difference between the observed incidence angle and the nominal incidence angle for each polarization (1). The adjustment factor is calculated using observations from NSCAT [28], which is a Ku-band fan-beam scatterometer that observed the surface at a range of incidence angles, using the Amazon basin as a calibration target region. Adjustments are determined for the $1^\circ \times 1^\circ$ regions for each polarization. The incidence adjustment is dependent on the global location, polarization, and the departure from the reference angle and is not dependent on the LTOD the measurement is made. Regionally specific calibrations are determined for the Amazon and Congo regions. Incidence adjustments to σ^0 rarely exceed 1 dB [see Fig. 5(a)], and the residual uncertainty is less than a few tenths of a decibel. Azimuthal variations in σ^0 vary depending on the region of the world but are small (less than a few tenths of a decibel) for the regions studied. Azimuth variations are accounted for using an adjustment based on a 10° azimuth bin median filter of QuikSCAT surface observations for the same day-of-year range for 2008 for the $1^\circ \times 1^\circ$ bins and regions. These adjustments remove azimuthal variations and incidence angle effects while leaving other signals such as the diurnal variation, i.e.,

$$\sigma^0_{adjusted} = \sigma^0_{measured} + (\theta_{measured} - \theta_{reference})K \quad (1)$$

where

$\sigma^0_{adjusted}$ adjusted σ^0 (dB),
$\sigma^0_{measured}$ measured σ^0 (dB),
$\theta_{measured}$ measured incidence angle,
$\theta_{reference}$ referenced nominal incidence angle (49° for HH and 56° for VV), and K is the scaling factor (dB/degree) for converting the difference in the incidence and reference angles into the required additive value for obtaining $\sigma^\circ_{adjusted}$.

While the nature of the ISS orbit does not support observations of the full diurnal cycle within a single day, the multiple LTOD observations spread over multiple days allow for observations to be composited to generate the full diurnal cycle by assuming a negligible seasonal cycle for the period of study. Making a composite diurnal signal from samples over multiple days at various times comes with the risk of aliasing into the composite diurnal other processes that might occur on impacting timescales such as a freeze-thaw event. The influence of freeze-thaw events is limited by the temperature and snow depth considerations previously described. To avoid large seasonal changes, the time period has been limited to less than three months when much of the vegetation in the Northern Hemisphere is dormant. Possible seasonal influences might still be present in selected parts of the globe; however, in this paper, we do not attempt to identify further seasonal changes in this analysis since a much longer time period is required for a thorough analysis. Other changes may impact the composite diurnal signal such as changes in canopy moisture. Other sources of variations may add noise to the data analysis. For example, due to short temporal duration and small spatial scale, rain can add a noise-like variation of up to several decibels to individual measurements. Cloud coverage and light precipitation are largely transparent to the Ku-band, and the effects are not distinguishable in the signal or data. The GLCC mask aids in identifying vegetation characteristics for these regions and the globe.

The LTOD observations for each grid element ($1^\circ \times 1^\circ$ bin) are separated into 16 temporal bins, each representing all of

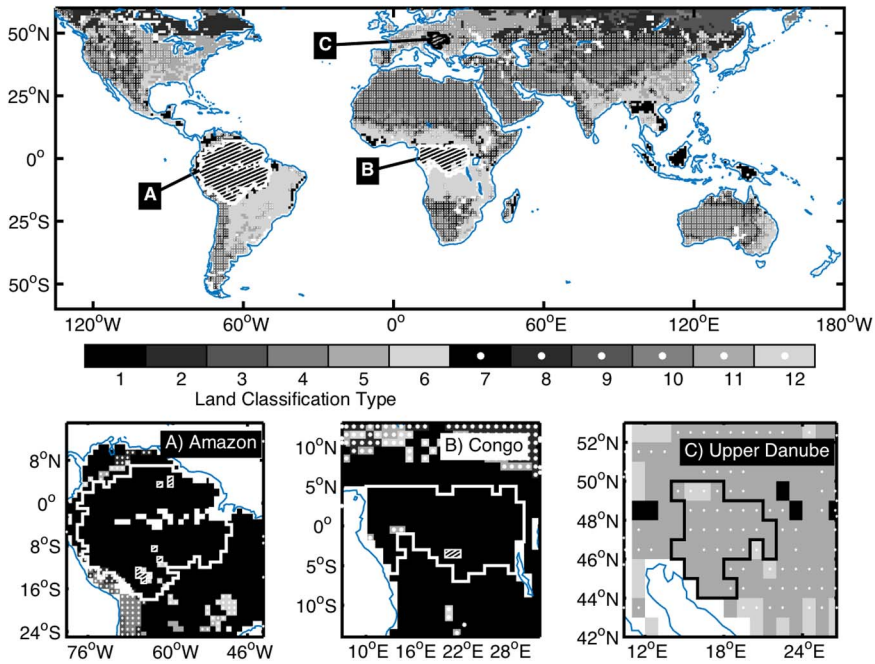

Fig. 4. Land classification type for the University of Maryland 1° AVHRR GLCC types with corresponding numerical identifiers as described in Table II for $1^\circ \times 1^\circ$ regions globally with five regions outlined for A—Amazon, B—Congo, and C—Upper Danube.

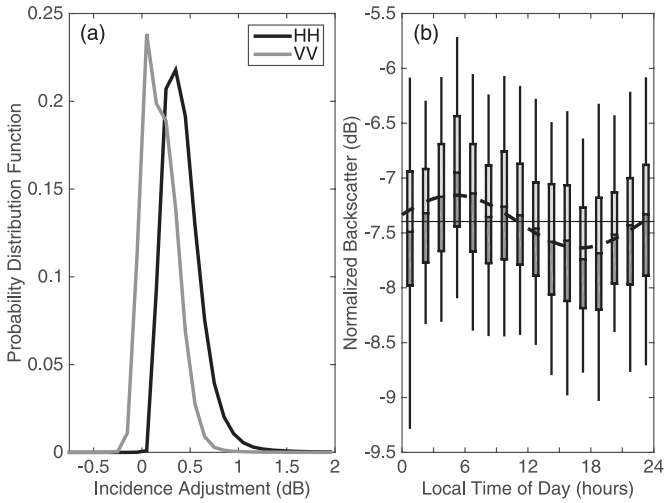

Fig. 5. (a) Probability distribution function of incidence adjustments to σ^0 for all RapidScat σ^0 observations for HH (black) and VV (gray). (b) Diurnal changes in 90-min LTOD bins for a $1^\circ \times 1^\circ$ region at 0°N and 100° E in Sumatra. Box-and-whisker plots identifying the 5th, 25th, 75th, and 95th percentiles and median for the 90-min bins, mean σ^0 (black solid line), and sinusoidal fit (black dashed line).

the LTOD observations for a 90-min window. The data in the top and bottom fifth percentiles are excluded when the mean for each bins is calculated. The maximum difference in the bin means (amplitude) is used to determine the extent of the diurnal change in backscatter. This analysis is also performed for the globe and for the large study regions: the Amazon, Congo, and Upper Danube river basin. Many other parts of the Earth demonstrate similar characteristics to these regions but do not have the same spatial extent with spatially consistent surface characteristics for the large scale for the analysis employed in this study.

In addition to determining the amplitude of the diurnal change, departures from the daily mean are identified. The departures from the mean appear as a sinusoidal-like pattern in the diurnal cycle with maxima occurring at different LTOD observations, depending on the region. A similar periodic diurnal cycle is observed over most of the global regions, although the pattern is not perfectly sinusoidal. To identify the extent of the diurnal signal, the LTOD bins for which the maximum and minimum binned means occur for each element are used to determine the time of the maximum and the time difference between the maximum and minimum values (dt). Time differences in the occurrences of the maximum and minimum less than 4 h indicate that changes in the diurnal signal do not follow a periodic pattern. The amplitude, LTOD of the maximum, and dt can be used to characterize the diurnal changes.

V. Results

The global mean backscatter over land as observed by RapidScat is −10.9 dB [see Fig. 6(a)]. Regions with vegetated ground cover have higher mean backscatter values, in general. Arid and semiarid regions tend to have lower backscatter with the exception of the deserts of the southwestern United States where sparse vegetation exists. Regions with low signal-to-noise ratio (SNR), such as the Sahara Desert, prohibit extensive analysis because of the lack of quality of the data. Not all similarly vegetated regions have the same mean backscatter.

The median diurnal backscatter variation is 1.05 dB globally. The changes in the diurnal backscatter signal are found to be over 4 dB for some regions, but over 90% of the diurnal changes are below 2.5 dB (see Fig. 7). Some large regions can be identified by similar diurnal changes, both in magnitude, the time of the maximum value, and dt [see Fig. 6(b) and (c)]. Regions with elevated diurnal variations as observed from the

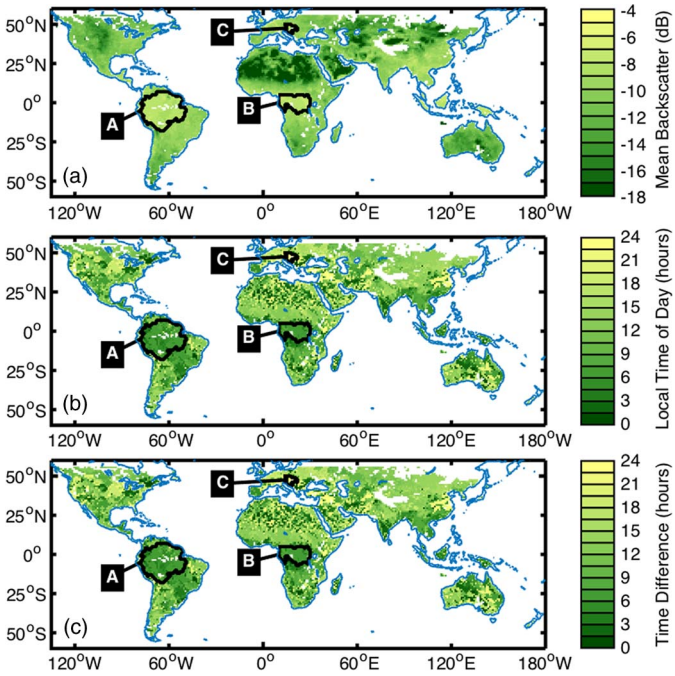

Fig. 6. (a) Mean σ^0 from RapidScat for $1^\circ \times 1^\circ$ regions globally with five regions outlined for A—Amazon, B—Congo, and C—Upper Danube. (b) Time occurrence the maximum binned mean. (c) Difference in time between the maximum and minimum binned means.

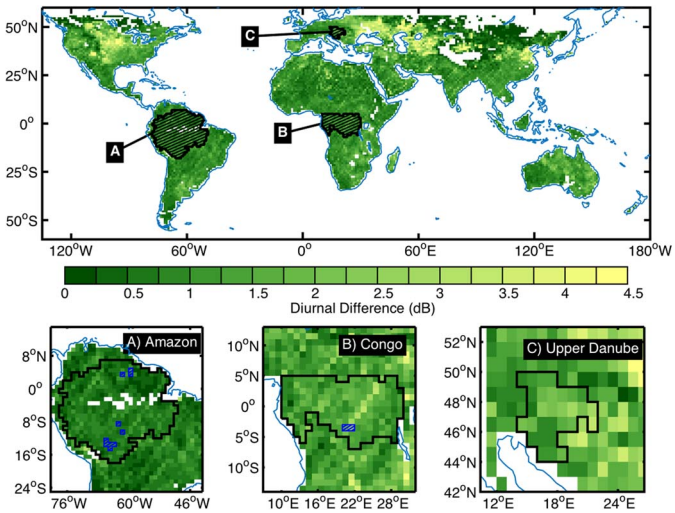

Fig. 7. (Top) Maximum differences in the diurnal signal from RapidScat HH σ^0 observations with five highlighted regions: (A) Amazon, (B) Congo, and (C) Upper Danube. Subregions in blue are not included in the regional analysis because of the requirements for establishing the regions.

6:00 A.M. and 6:00 P.M. LTOD observations from QuikSCAT, such as from northern South America and central Africa (see Fig. 1), also appear in the diurnal variations calculated from the RapidScat data; however, other areas with little to no diurnal change in the QuikSCAT observations have a notable change in the RapidScat observations, which is probably due to the QuikSCAT sampling time of the phase of the diurnal cycle.

For parts of the globe, the maximum and minimum of the diurnal change occurs approximately 12 h apart. Sun-synchronous satellites such as QuikSCAT can only observe a mid-latitude to a low-latitude location twice daily. If the observations occur at the maximum and minimum of the diurnal change, the difference is representative of the amplitude of the diurnal change; however, when the observations do not occur at the maximum and minimum, the difference does not represent the amplitude of the diurnal change [see Fig. 5(b)]. The unique orbit of the ISS and RapidScat allows for observations at different LTODs to composite the full diurnal pattern.

The diurnal cycle around the globe can be described by either a sinusoidal-like pattern for regions with at least 6 h between the daily maximum and minimum mean backscatter observations (or less than 18 h depending on the time of the maximum) or no distinct pattern for the other regions. The sinusoidal-like pattern appears periodic, but is not necessarily described with a simple sinusoidal function; however, the mean backscatter, time occurrence of the maximum binned mean observation, the amplitude, and dt are useful to describe the diurnal cycles and to identify regions with similar patterns. For example, the Congo and Amazon regions are highly correlated to areas of the globe such as the northern Indochinese Peninsula and the upper Guinean forests. All these regions exhibit a similar LTOD maximum and similar dt. Much of the observed globe can be characterized with these three diagnostic traits. Some regions, particularly desert regions, either do not have notable or describable diurnal backscatter changes or the signal cannot be distinguished from the natural variability and system noise. Some other regions could not be analyzed because of the limited data availability after filtering for freeze/thaw cycles. We focus on three regions in this analysis; the regions listed are examples and should not be considered an exhaustive list of the possible observed diurnal cycles or lack thereof.

A. *Amazon Region*

The Amazon region has been used as a land calibration target for cross-calibrating several sensors [5], [23], [24] because of the large-scale uniformity in the backscatter response from the vegetation in the region. However, variations in the backscatter caused by LTOD effects have been problematic for cross-sensor calibration [5]. The RapidScat observations identify a 0.55 (0.57)-dB mean change for HH (VV) in the diurnal signal for the Amazon region with the morning backscatter response being larger than evening for both polarizations and the ascending and descending paths [see Fig. 8(a)]. The change in the diurnal signal for QuikSCAT is 0.47 (0.48) dB for HH (VV) for comparison. The overall mean for RapidScat is -8.03 (-9.36) dB for HH (VV). The maximum diurnal signal occurs around 6:00 A.M. LTOD and a dt of about 12 h for the region on average. A sinusoidal-like pattern is evident in the signal for the region, but the amplitude is smaller than the standard deviation of the data. The surface cover is dominantly characterized by Broadleaf Evergreen Forest with some smaller portions, including Wooded Grassland, Grassland, and Broadleaf Deciduous Forest and Woodland.

B. *Congo Region*

The Congo region also has a morning maximum with a dt around 12 h similar to the Amazon region except that the

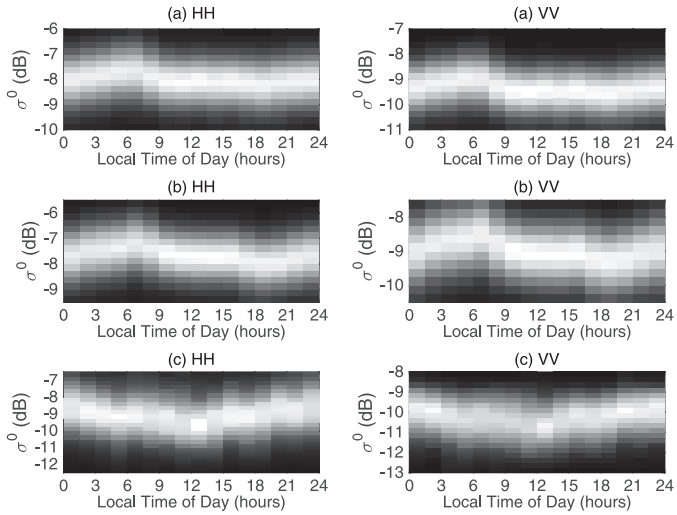

Fig. 8. Probability distribution function in two dimensions of the distribution of RapidScat σ^0 observations for LTOD (90-min bins) for HH (left) and VV (right). (A) Amazon, (B) Congo, and (C) Upper Danube. The shades of gray represent the number of occurrences (the lighter the gray, the more occurrences).

offset is higher and the amplitude is greater. The diurnal signal difference is 0.77 (0.79) dB for HH (VV) with the morning backscatter response also being larger than the evening [see Fig. 8(b)]. The change in the diurnal signal for QuikSCAT is 0.67 (0.61) dB for HH (VV) for comparison. The overall mean for RapidScat is -7.66 (-8.98) dB for HH (VV). The surface cover is dominantly characterized by Broadleaf Evergreen Forest with some smaller portions, including Wooded Grassland and Cultivated Crops.

C. Upper Danube River Region

In the Upper Danube river region, a similar dt of about 12 h also appears at different pattern appears, but the maximum occurs after midnight LTOD. The Upper Danube river region encompasses countries such as Turkey, Austria, and Slovakia. The diurnal mean signal change from RapidScat is 1.21 (0.83) dB for HH (VV) from the -9.77 (-10.71)-dB mean value [see Fig. 8(c)], whereas the QuikSCAT diurnal change is only 8.1×10^{-2} (0.10) dB for HH (VV). The vegetation in the region is largely cropland with some Broadleaf Deciduous Forest and Woodland and Mixed Coniferous Forest and Woodland, although the cropland during the time period of study is likely to be harvested or dormant.

VI. Discussion

RapidScat observations enable the study of the diurnal changes to the backscatter signal on a global scale. The unique mission of RapidScat aboard the ISS provides a context for cross-calibrating other instruments that did not operate simultaneously or that collected observations at different LTODs. The non-sun-synchronous orbit of the ISS with a changing LTOD surface observation allows for a composite analysis of the LTOD within approximately 1 h roughly every two months when considering the ascending and descending passes separately and roughly every 22 days by combining the ascending and descending passes. The full diurnal cycle can be observed on the subseasonal timescale. The ISS orbit limits global coverage daily to between 58° S and 58° N.

The diurnal cycle has been previously studied, and the backscatter cycle has been theorized, but only now does definitive evidence exist about the diurnal changes in the surface backscatter response for large-scale regional areas. Regional responses vary around the globe, but no single diurnal pattern exists for all regions or even across similar vegetation types. This discovery confirms many of the findings of previous regional studies and provides further insight for future research.

We observe that diurnal cycles exist beyond the cycles previously studied. The maximum and minimum values tend to occur approximately 12 h apart for regions with a notable diurnal signal, and the diurnal changes can be qualitatively described by the overall mean value, amplitude, the LTOD when the maximum occurs, and dt. Vegetated regions tend to experience a diurnal change; however, specific types of vegetation do not determine the extent of changes. Possible diurnal changes in arid regions with minimal vegetation, such as deserts, cannot be clearly defined because of the lower SNR in these regions, but with more observations, the desert diurnal signal might be discernable. Seasonal changes to the surface such as crop growth and harvesting are known to impact the backscatter signal [18], and a longer data record is required to analyze these changes over multiple seasons and regions. We postulate that vegetation type and other factors such as soil moisture, terrain, soil type, season, and phenological processes or regional vegetation can likely be used to describe the diurnal changes observed by RapidScat with future study.

The regional diurnal signals as observed from RapidScat can be used to cross-calibrate other scatterometers using a similar frequency regardless of the equatorial cross times for similar seasons and with the data constraints used in this study. The RapidScat data and diurnal analysis can be used as a common reference metric for regions such as the Amazon and Congo. For example, observations from NSCAT and OSCAT with different equatorial cross times can be compared using the RapidScat diurnal cycle as a common reference. Unfortunately, the ISS orbit prevents calibration in the polar regions, but the potential exists to analyze seasonal snow events in parts of southern Canada and throughout northern Europe and Asia. We defer such calibration issues to future work.

However, the diurnal variations from the mean σ^0 as observed from RapidScat and QuikSCAT can be compared globally without additional discussion of instrument cross-calibration (see Fig. 9). Regions where the extrema of the local sinusoidal phase as observed from RapidScat closely match the observation times of QuikSCAT have similar magnitudes of changes in the diurnal signal. The diurnal variation from the mean as observed by RapidScat is contained within the QuikSCAT observations that are adjusted to a zero mean for the Amazon and Congo regions. The similar diurnal variations validate previous research for these regions. QuikSCAT does not provide observations at the diurnal extrema for every region, and the regions with diurnal extrema that are well described using QuikSCAT are limited. Sensors with different equatorial cross times will provide better observations of the diurnal

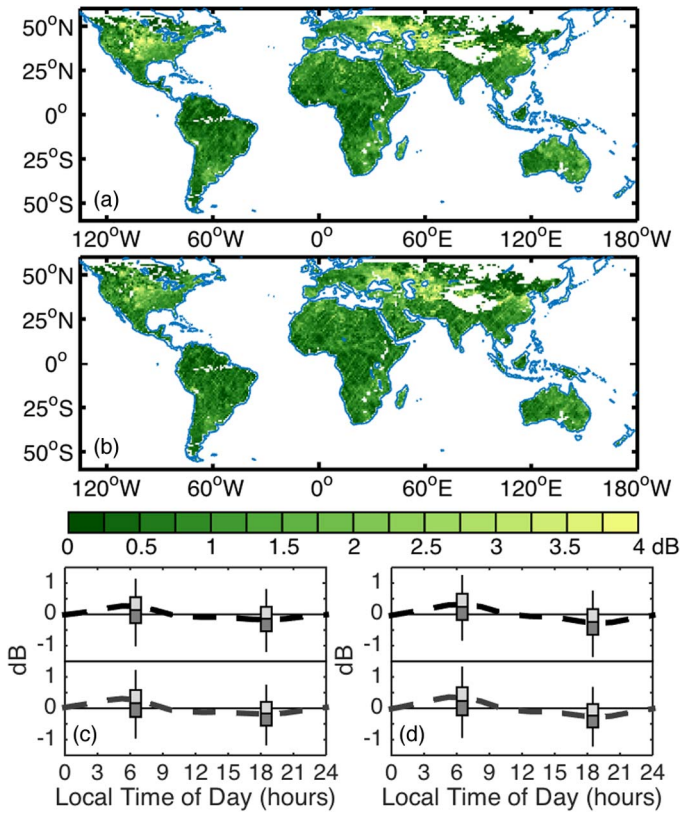

Fig. 9. (a) Absolute difference in the magnitude of the observed diurnal signal from RapidScat and QuikScat for HH. (b) Absolute difference in the magnitude of the observed diurnal signal from RapidScat and QuikScat for VV polarization. (c) Diurnal changes from the zero mean σ^0 value for RapidScat (dashed line) and QuikSCAT (box-and-whisker plots identify the 5th, 25th, 75th, and 95th percentiles and median) for HH (top) and VV (bottom). (d) Diurnal changes from the zero mean σ^0 value for RapidScat (dashed line) and QuikSCAT (box-and-whisker plots identify the 5th, 25th, 75th, and 95th percentiles and median) for HH (top) and VV (bottom).

extrema for different regions. Analyzing the diurnal variations using multiple sun-synchronous scatterometers will require further instrument cross-calibration, and one single region, such as the Amazon, cannot provide both mean and extrema comparisons across all sensors without a common reference such as RapidScat. Comparison and cross-calibration of RapidScat to other Ku-band scatterometers are left for future research.

This analysis has been performed for multiple regional scales. Sub $1^\circ \times 1^\circ$ scales were also analyzed (not shown), but the spatial scales of the surface observations and the lack of an extended time record limit the analysis. A longer data record will be useful in analyzing seasonal changes and the diurnal cycle, but a longer data record requires the analysis of both the seasonal change and diurnal cycle as the seasonal changes for much of the land surface are of larger amplitude than the diurnal effects. In essence, to account for the diurnal effects and seasonal effects with observations from RapidScat, both effects must be accounted for in a period shorter than two months or when the local seasons and vegetation are quickly changing. Analyzing changes on smaller spatial scales is possible with observations of sufficient quality.

The diurnal response of specific vegetation type and land use all likely play a role in determining the backscatter response and any diurnal variations. The nonlinear processes in the Calvin cycle [29], which describes the chemical processes in photosynthesis, and the soil–plant–atmosphere continuum [30], which describes water transport through a plant, might be key in describing and predicting the backscatter response for vegetated regions. A future analysis including plant life cycles, density, and available moisture is necessary to account for these possible effects on the diurnal changes in a region. Other surface modifications, such as the presence of snow or different types of tree undergrowth, might also impact the signal.

RapidScat provides our first look into the diurnal variations in the observed σ^0 from a single platform and can be used as a common metric against which previous and future Ku-band scatterometers can be calibrated for multisensor studies. The temporal gaps in the composite diurnal coverage made over the period of a month are small compared with the gaps that previously existed using multiple sensors such as QuikSCAT and OSCAT. RapidScat data cannot be used to analyze the temporal variations within a single day; hence, possible signal aliasing must be considered in using the data for scientific research. Even with these limitations, RapidScat is providing valuable insight of the diurnal cycle observed globally and is providing useful information for improvements for future instrument and orbit design.

VII. Conclusion

Diurnal changes in the backscatter signal exist around the globe, and the diurnal changes vary over regions. Four distinct sinusoidal-like phases of the diurnal signal have been identified from the data. Some parts of the globe exhibit similar changes on a larger scale that can be correlated with vegetation; however, no clear causality is identified. The findings support the theory of the vegetation moisture processes in the Amazon and Congo regions, but other regions identified showed different phases of a diurnal cycle that are not necessarily consistent with the cycle previously identified for the Amazon and Congo and the circadian processes associated with similar vegetation and available moisture. Further research regarding the regional vegetation type, season, available soil moisture, and phenological processes including the Calvin cycle and moisture in the soil–plant–atmosphere continuum of the local vegetation is needed to identify the primary cause of the diurnal changes. Additionally, changes to the ground cover by snow and ice or other changes have not yet been characterized with the data currently available. As the RapidScat mission progresses and more data become available, the changes due to ground cover can be more thoroughly analyzed.

Acknowledgment

The authors would like to thank NASA, the Jet Propulsion Laboratory, and those that made RapidScat possible.

References

[1] R. G. Kennett and F. K. Li, "Seasat over-land scatterometer data, Part 1. Global overview of the Ku-band backscatter coefficients," *IEEE Trans. Geosci. Remote Sens.*, vol. 27, no. 5, pp. 592–605, Sep. 1989.

[2] R. G. Kennett and F. K. Li, "Seasat over-land scatterometer data, Part 2. Selection of extended area land-target sites for the calibration of spaceborne scatterometers," *IEEE Trans. Geosci. Remote Sens.*, vol. 27, no. 5, pp. 779–788, Sep. 1989.

[3] J. S. Friesen, S. C. Steele-Dunne, and N. van de Giesen, "Diurnal differences in global ERS backscatter," *IEEE Trans. Geosci. Remote Sens.*, vol. 50, no. 7, pp. 2595–2602, Jul. 2012.
[4] S. C. Steele-Dunne, J. S. Friesen, and N. van de Giesen, "Using diurnal variation in backscatter to detect vegetation water stress," *IEEE Trans. Geosci. Remote Sens.*, vol. 50, no. 7, pp. 2618–2629, Jul. 2012.
[5] D. G. Long, "Comparison of TRMM and NSCAT observations of surface backscatter over the Amazon rain forest," in *Proc. IEEE IGARSS*, 1998, pp. 1879–1881.
[6] C. Kummerow, W. Barnes, T. Kozu, J. Shiue, and J. Simpson, "The Tropical Rainfall Measuring Mission (TRMM) sensor package," *J. Atmos. Ocean. Technol.*, vol. 15, no. 3, pp. 809–817, Jun. 1998.
[7] X. T. Liu, Y. F. Fu, and Q. Liu, "Significant impacts of the TRMM satellite orbit boost on climatological records of tropical precipitation," *Chin. Sci. Bull.*, vol. 57, no. 35, pp. 4627–4634, Dec. 2012.
[8] V. M. Cooley, "Unique offereings of the ISS as an Earth observing platform," in *Proc. 64th Int. Astron. Congr.*, Beijing, China, pp. 1–6, Sep. 2013, IAC-13-D9.2.8.
[9] E. Rodriguez, "The NASA ISS-RapidScat mission (Invited)," presented at the American Geophysical Union Fall Meeting, San Francisco, CA, USA, Dec. 9–13, 2013, Paper U23A-03.
[10] M. H. Freilich, D. G. Long, and M. W. Spencer, "SeaWinds: A scanning scatterometer for ADEOS II-science overview," in *Proc. IGARSS*, Aug. 8–12, 1994, vol. 2, pp. 960–963.
[11] W.-T. Tsai, M. Spencer, C. Wu, C. Winn, and K. Kellogg, "SeaWinds on QuikSCAT: Sensor description and mission overview," in *Proc. IGARSS*, Jul. 24–28, 2000, vol. 3, pp. 1021–1023.
[12] L. A. Jones *et al.*, "Satellite microwave remote sensing of daily land surface air temperature minima and maxima from AMSR-E," *IEEE J. Sel. Topics Appl. Earth Observ. Remote Sens.*, vol. 3, no. 1, pp. 111–123, Mar. 2010.
[13] H. Norouzi *et al.*, "Using microwave brightness temperature diurnal cycle to improve emissivity retrievals over land," *Remote Sens. Environ.*, vol. 123, pp. 470–482, Aug. 2012.
[14] K. Y. Vinnikov, Y. Yu, M. K. Rama Varma Raja, D. Tarpley, and M. D. Goldberg, "Diurnal-seasonal and weather-related variations of land surface temperature observed from geostationary satellites," *Geophys. Res. Lett.*, vol. 35, no. 22, Nov. 2008, Art. ID L22708.
[15] I. J. Birrer, E. M. Bracalente, G. J. Dome, J. Sweet, and G. Berthold, "σ^0 signature of the Amazon Rainforest obtained from the Seasat scatterometer," *IEEE Trans. Geosci. Remote Sens.*, vol. GE-20, no. 1, pp. 11–17, Jan. 1982.
[16] M. Satake and H. Hanado, "Diurnal change of Amazon rain forest observed by Ku-band spaceborne radar," *IEEE Trans. Geosci. Remote Sens.*, vol. 42, no. 6, pp. 1127–1134, Jun. 2004.
[17] S. Frolking *et al.*, "Evaluation of the SeaWinds scatterometer for regional monitoring of vegetation phenology," *J. Geophys. Res.*, vol. 111, no. D17, Sep. 2006, Art. ID D17302.
[18] A. C. Paget, S. Frolking, D. G. Long, and T. Milliman, "Satellite radar anisotropy observed in urban areas," *Int. J. Remote Sens.*, vol. 36, no. 2, pp. 665–679, Jan. 2015.
[19] N. M. Madsen and D. G. Long, "Calibration and validation of the RapidScat scatterometer using tropical rainforests," *IEEE Trans. Geosci. Remote Sens.*, vol. 54, no. 5, pp. 2846–2854, May 2016.
[20] D. G. Long and P. J. Hardin, "Vegetation studies of the Amazon Basin using enhanced resolution Seasat scatterometer data," *IEEE Trans. Geosci. Remote Sens.*, vol. 32, no. 2, pp. 449–460, Mar. 1994.
[21] H. Stephen and D. G. Long, "Multi-spectral analysis of the Amazon basin using SeaWinds, ERS, Seasat scatterometers, TRMM-PR and SSM/I," in *Proc. IEEE IGARSS*, Jun. 24–28, 2002, vol. 3, pp. 1780–1782.
[22] R. Crapolicchio and P. Lecomte, "On the stability of Amazon rainforest backscattering during the ERS-2 scatterometer mission lifetime," in *Proc. Envisat/ERS Symp.*, 2004, pp. 1–8.
[23] J. Zec, D. G. Long, and W. L. Jones, "NSCAT normalized radar backscattering coefficient biases using homogenous land targets," *J. Geophys. Res.*, vol. 104, no. C5, pp. 11 557–11 568, May 1999.
[24] D. G. Long and G. B. Skouson, "Calibration of the spaceborne scatterometers using tropical rain forest," *IEEE Trans. Geosci. Remote Sens.*, vol. 34, no. 2, pp. 413–424, Mar. 1996.
[25] L. B. Kunz and D. G. Long, "Calibrating SeaWinds and QuikSCAT scatterometers using natural land targets," *IEEE Geosci. Remote Sens. Lett.*, vol. 2, no. 2, pp. 182–186, Apr. 2005.
[26] P. Hailong, M. Bo, L. Mingsen, and Z. Wu, "HY-2A satellite calibration and validation approach and results," in *Proc. IEEE IGARSS*, Jul. 13–18, 2014, pp. 4528–4531.
[27] S. Jaruwatanadilok and B. W. Stiles, "Trends and variation in Ku-band backscatter of natural targets on land observed in QuikSCAT data," *IEEE Trans. Geosci. Remote Sens.*, vol. 52, no. 7, pp. 4383–4390, Jul. 2014.
[28] F. M. Naderi, M. H. Freilich, and D. G. Long, "Spaceborne radar measurement of wind velocity over the ocean—An overview of the NSCAT scatterometer system," *Proc. IEEE*, vol. 79, no. 6, pp. 850–866, Jun. 1991.
[29] C. A. Raines, "The Calvin cycle revisited," *Photosynthesis Res.*, vol. 75, no. 1, pp. 1–10, Jan. 2003.
[30] M. Williams *et al.*, "Modelling the soil–plant–atmosphere continuum in a Quercus-Acer stand at Harvard Forest: The regulation of stomatal conductance by light, nitrogen and soil/plant hydraulic properties," *Plant, Cell Environ.*, vol. 19, no. 8, pp. 911–927, Aug. 1996.

Aaron C. Paget (M'13) received the M.S. degree in meteorology and the Ph.D. degree in geophysical fluid dynamics from the Florida State University, Tallahassee, FL, USA, in 2010 and 2013, respectively.

From 2013 to 2015, he was a Postdoctoral Fellow with the Microwave Earth Remote Sensing Laboratory, Brigham Young University, Provo, UT, USA, where he developed remote sensing data processing techniques to analyze microwave remote sensing data from scatterometers for land and ocean analysis. He is currently a Postdoctoral Fellow with the Department of Marine Sciences, University of Connecticut, Storrs, CT, USA. His research interests include boundary-layer processes, satellite remote sensing, *in situ* instrumentation, coupled modeling, oceanic whitecap generation, and air–land and air–sea interaction.

David G. Long (S'80–SM'98–F'08) received the Ph.D. degree in electrical engineering from the University of Southern California, Los Angeles, CA, USA, in 1989.

From 1983 to 1990, he worked for NASA's Jet Propulsion Laboratory (JPL) where he developed advanced radar remote sensing systems. While at JPL, he was the Project Engineer on the NASA Scatterometer (NSCAT) project, which flew from 1996 to 1997. He also managed the SCANSCAT project, the precursor to SeaWinds, which was flown in 1999 on QuikSCAT, in 2002 on ADEOS-II, and in 2014 on the International Space Station. He is currently a Professor with the Department of Electrical and Computer Engineering, Brigham Young University (BYU), Provo, UT, USA, where he teaches upper division and graduate courses in communications, microwave remote sensing, radar, and signal processing and is the Director of the BYU Center for Remote Sensing. He is the Principal Investigator on several NASA-sponsored research projects in remote sensing. He has over 400 publications in various areas, including signal processing, radar scatterometry, and synthetic aperture radar. His research interests include microwave remote sensing, radar theory, space-based sensing, estimation theory, signal processing, and mesoscale atmospheric dynamics.

Dr. Long has received the NASA Certificate of Recognition several times and is an Associate Editor of the IEEE GEOSCIENCE AND REMOTE SENSING LETTERS.

Nathan M. Madsen (M'15) received the M.S. degree in electrical engineering from Brigham Young University, Provo, UT, USA, in 2015.

While there, he performed research with the BYU Microwave Earth Remote Sensing Laboratory. He recently joined Rincon Research Inc., Tucson, AZ, USA.